WMO Provisional State of the Global Climate 2022

WORLD METEOROLOGICAL ORGANIZATION

Contents

Highlights

Concentrations of the three main greenhouse gases – carbon dioxide, methane, and nitrous oxide – reached record highs in 2021. The annual increase in methane concentration was the highest on record. Real time data from specific locations show levels of the three gases continued to increase in 2022.

Global mean temperature in 2022 is currently estimated to be 1.15 ± 0.13 °C above the 1850-1900 average. The eight years 2015 to 2022 are likely to be the eight warmest years on record, with 2022 most likely to be 5th or 6th warmest.

La Niña conditions have continued with short interruptions since late 2020 and are expected to continue through late 2022. This would mark the third consecutive year of La Niña. Such a triple-dip La Niña is unusual and has kept global temperature low for the second year in a row.

Sea level continued to rise in 2022, reaching a new record high. Since January 2020, global mean sea level has risen by nearly 10mm, approximately 10% of the overall rise in sea level since satellite measurements began in 1993.

A low winter snowpack in 2021/22 combined with an exceptionally warm summer in Europe led to record glacier mass losses in Switzerland with 6% of the glacier ice volume lost between 2021 and 2022. Between 2001 and 2022 the volume of glacier ice in Switzerland decreased from 77 km^3 to 49 km^3, a decline of more than a third.

In east Africa, rainfall has been below average in four consecutive wet seasons, the longest sequence in 40 years with early indications that the current season could also be drier than average. Across the region, under the effects of the drought and other shocks, an estimated 18.4 to 19.3 million people have faced food Crisis or worse levels of acute food insecurity before June 2022.

Record breaking rain in July and August led to extensive flooding in Pakistan. There were at least 1 700 deaths and 33 million people affected. 7.9 million people were displaced.

Record breaking heatwaves affected China and Europe during the summer coupled with exceptionally dry conditions in places.

The southern Africa region has been battered by a series of cyclones over two months, leading to a surge in the need for protection and shelter for hundreds of thousands of affected persons.

Executive Summary

The State of the Global Climate in 2022 is produced on an annual basis, complementing the most recent long assessment cycle provided by the sixth IPCC Assessment Report. This is the provisional version; the full and final report is expected to be published in March 2023. The report provides an authoritative voice on the current state of the climate using key climate indicators and reporting on extreme events and their impacts. Collecting and analysing data from these variables takes time—where 2022 data is not yet available, figures from 2021 are provided.

In 2021, concentrations of the three main greenhouse gases – carbon dioxide, methane, and nitrous oxide – continued to reach record highs. The annual increase in methane concentration was the highest on record, which is especially significant given that methane is more than 25 times more potent than carbon dioxide at trapping heat in the atmosphere. Real time data from specific locations show levels of the three gases continued to increase in 2022.

The impact of increased concentration of GHG in the atmosphere is first and foremost on global temperatures. Global mean temperature in 2022 is currently estimated to be 1.15 ± 0.13 °C above the pre-industrial (1850-1900) average, likely making the past eight years (2015-2022) the warmest on record. Despite La Niña conditions keeping global temperature low for the second consecutive year, 2022 is still most likely to be 5th or 6th warmest year on record.

Rising global temperatures have impacts on both the sea and on land. Antarctic sea-ice extent reached a record low in February 2022, at almost 1 million km^2 below the long-term mean. Meanwhile, the ocean continued to warm in 2021 and is expected to continue to warm well into the future. As the ocean warms, it expands, contributing to global sea level rise. Sea level continued to rise in 2022, reaching record high levels. Since January 2020, global sea level has risen nearly 10mm. Although this may not sound significant, it represents approximately 10% of the overall rise in sea level since satellite measurements began in 1993 in only 2 years, indicating that the rate of rise is speeding up.

As temperatures rise, the continued melting of ice over land around the world is further contributing to accelerating sea level rise. The Greenland Ice Sheet ended with a negative total mass balance for the 26th year in a row. Meanwhile, in Switzerland, 6% of the glacier ice volume was lost between 2021 and 2022, following low winter snowpack, dust coatings from the Sahara and an exceptionally warm summer in Europe. Between 2001 and 2022 the volume of glacier ice in Switzerland decreased from 77 km^3 to 49 km^3, a decline of more than a third.

Weather and climate extremes and their induced impacts are also exacerbated by rising global surface and sea temperatures. In East Africa, rainfall has been below average for four consecutive wet seasons, the longest sequence in 40 years. Across the region, under the effects of the drought and other shocks, an estimated 18.4-19.3 million people were facing acute food insecurity. In Pakistan, record breaking rain in July and August led to extensive flooding and approximately 1700 deaths, with 7.9 million people displaced, and 33 million people affected.

Large parts of the northern hemisphere were exceptionally hot and dry in 2022. China had the most extensive and long-lasting heatwave since national records began and the second-driest summer on record. The Yangtze River at Wuhan reached its lowest recorded level for August. The temperature exceeded 40 °C in the United Kingdom for the first time, with a reading of 40.3 °C at Coningsby on 19 July, 1.6 °C above the previous national record. The heat extended as far north as Sweden, where 37.2 °C at Målilla on 21 July was the country's highest since 1947. Drought conditions were at their most severe in August, when rivers including the Rhine, Loire and Danube fell to critically low levels.

Taken together, these changes to the global climate are undermining the global ability to achieve sustainable development, directly impacting Sustainable Development Goals 1,2, 3, 6, 7, 10, 13, 14 and 15. However, the picture is far from complete. Significant gaps still exist for many key climate parameters, including ocean acidification (SDG 14) and methane emissions (SDG 13). Filling these gaps is essential for understanding the interconnections between climate change and development, and better addressing the disparities of where impacts are being felt, improving adaptation, and urging rapid mitigation.

Global Climate Indicators

The global climate indicators provide an overview of changes in the climate system at the broadest scale[1]. This set of interlinked physical indicators connects the changing composition of the atmosphere with changes in energy in the climate system and the response of land, ocean, and ice.

The global indicators are based on a wide range of data sets which are, in turn, based on multiple observing systems including both satellite and in situ data sources. For a complete list of datasets and information on baselines used in the report, see Data sets and methods.

Baselines

Baselines are periods of time, usually spanning one or more decades, that are used as a fixed benchmark against which conditions can be compared. Different baselines are used in this report, and these are specified in the text and figures. Where possible, the WMO climatological standard normal, 1981-2010, is used for consistent reporting. For some indicators, however, this is not possible owing to a lack of measurements during the early part of the period, or because a longer period is required to calculate representative statistics (for example, for precipitation).

There are two exceptions. First, for the global mean temperature time series – and only for the global mean series – a reference period of 1850-1900 is used. This is the baseline used in the recent IPCC reports as a reference period for pre-industrial conditions and is relevant for understanding progress in the context of the Paris Agreement. Second, greenhouse gas concentrations can be estimated much further back in time using gas bubbles trapped in ice cores. The year 1750 is therefore used in this report to represent pre-industrial greenhouse gas concentrations.

Greenhouse gases

Atmospheric concentrations of greenhouse gases reflect a balance between emissions from human activities, natural sources, and sinks in the biosphere and ocean. Increasing levels of greenhouse gases in the atmosphere due to human activities are the major driver of climate change since the industrial revolution. Global average mole fractions of greenhouse gases – the concentration in the atmosphere – are calculated from in situ observations made at multiple sites in the Global Atmosphere Watch (GAW) Programme of WMO and partner networks.

Real-time data from specific locations, including Mauna Loa[2] (Hawaii) and Kennaook/Cape Grim[3] (Tasmania) indicate that levels of CO_2, CH_4 and N_2O reached record levels in 2022. In 2021 – the latest year for which consolidated global figures are available – atmospheric levels of greenhouse gases reached new highs (Figure 1), with globally averaged surface mole fractions for carbon dioxide (CO_2) at 415.7 ± 0.2 parts per million (ppm), methane (CH_4) at 1908 ± 2 parts per billion (ppb) and nitrous oxide (N_2O) at 334.5 ± 0.1 ppb, respectively, 149%, 262% and 124% of pre-industrial (1750) levels.

The increase in CO_2 from 2020 to 2021 was equal to that observed from 2019 to 2020, but higher than the average annual growth rate over the last decade. While the long-term increase in CO_2 is due to human emissions, year-to-year variations in the rate are largely associated with natural variability in the land and ocean carbon sinks. The record annual increase in 2016 was associated with the strong 2015/16 El Niño.

[1] Trewin, B., Cazenave, A., Howell, S., Huss, M., Isensee, K., Palmer, M. D., Tarasova, O., & Vermeulen, A. (2020). Headline indicators for global climate monitoring, Bulletin of the American Meteorological Society. https://doi.org/10.1175/BAMS-D-19-0196.1

[2] www.esrl.noaa.gov/gmd/ccgg/trends/mlo.html

[3] https://www.csiro.au/greenhouse-gases/

The annual increase of CH_4 was 18 ppb from 2020 to 2021. This is the largest increase on record and its causes are still being investigated. Measurements of the atmospheric CH_4 burden and its stable carbon isotope ratio $^{13}C/^{12}C$ suggest the largest contribution to the renewed increase in CH_4 since 2007 comes from microbial/biogenic sources, but the relative roles of anthropogenic and natural sources are unclear[4,5]. Filling gaps in the observations in climate sensitive areas like tropical wetlands is a way to improve understanding of the processes that drive changes in greenhouse gases and to use this knowledge to support efficient mitigation strategies.

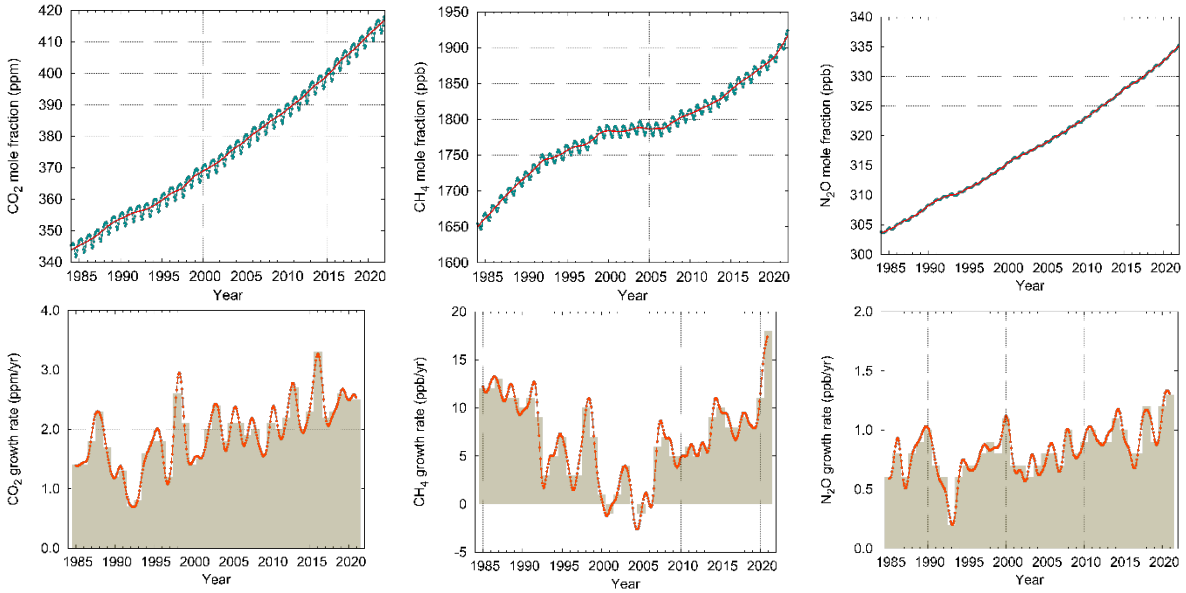

Figure 1: Top row: Globally averaged mole fraction (measure of atmospheric concentration), from 1984 to 2021, of CO_2 in parts per million (left), CH_4 in parts per billion (centre) and N_2O in parts per billion (right). The red line is the monthly mean mole fraction with the seasonal variations removed; the blue dots and line show the monthly averages. Bottom row: the growth rates representing increases in successive annual means of mole fractions for CO_2 in parts per million per year are shown as grey columns (left), CH_4 in parts per billion per year (centre) and N_2O in parts per billion per year (right) (Source: WMO Global Atmosphere Watch).

Global temperature

The global mean temperature so far in 2022 has been 1.15 [1.02 to 1.28] °C above the 1850-1900 average (Figure 2, 2022 figures are based on data from January to September). If the current anomaly continues to the end of the year, the six data sets used in the analysis would place 2022 as either the 5th or 6th warmest year on record (from 1850), and in each case marginally warmer than 2021. The eight years 2015 to 2022 are likely to be the eight warmest years on record in all data sets.

[4] Lunt, M. F., Palmer, P. I., Feng, L., Taylor, C. M., Boesch, H., and Parker, R. J. (2019): An increase in methane emissions from tropical Africa between 2010 and 2016 inferred from satellite data, Atmos. Chem. Phys., 19, 14721–14740, https://doi.org/10.5194/acp-19-14721-2019.
[5] Feng, L., Palmer, P. I., Zhu, S., Parker, R. J., & Liu, Y. (2022). Tropical methane emissions explain large fraction of recent changes in global atmospheric methane growth rate. Nature Communications, 13(1), 1–8. https://doi.org/10.1038/s41467-022-28989-z.

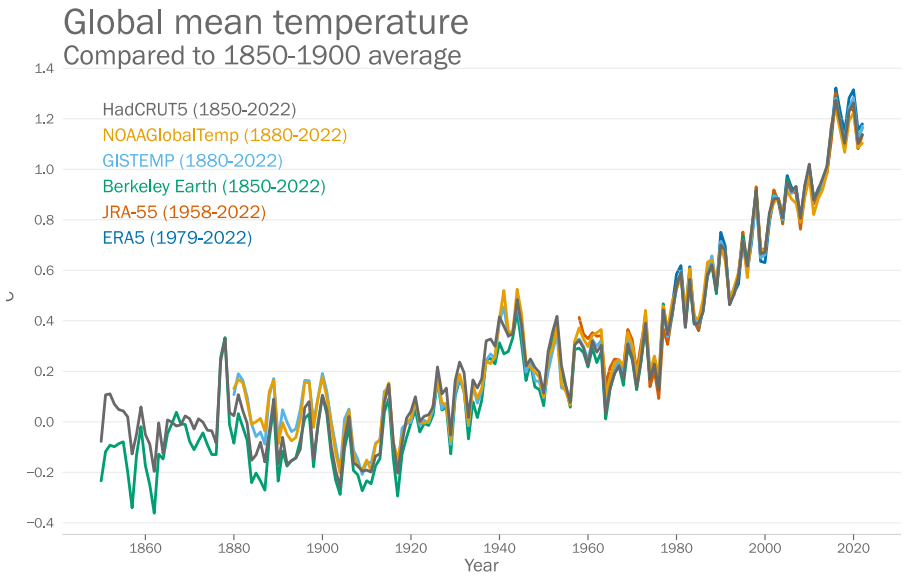

Figure 2: Global annual mean temperature difference from pre-industrial conditions (1850–1900) for six global temperature data sets (1850–2022, 2022 based on an average to September). For details of the data sets and processing see Data sets and methods.

La Niña conditions, which are associated with a temporary reduction in global temperature, have continued with short interruptions from late 2020 to present. La Niña conditions are expected to continue through late 2022[6] and would mark the third consecutive year of La Niña (see Short-term climate drivers). 2022 and 2021 both show a clear cooling effect from the ongoing La Niña conditions. Nonetheless, both years are warmer than 2011 (which had an anomaly of 0.87 [0.74 to 0.99] °C), the previous year affected by a significant La Niña event, and indeed any year prior to 2015. 2016, which was associated with an exceptionally strong El Niño, remains the warmest year on record globally (with an anomaly of 1.28 [1.15 to 1.40] °C) in most of the data sets surveyed.

In the IPCC sixth assessment report, long-term warming was assessed using multi-year averages[7]. For the period 2011–2020, the average anomaly was estimated to be 1.09 [0.95 to 1.20] °C. The 10-year average for the period 2013-2022 based on the data sets used here, is estimated to be 1.14 [1.02 to 1.27] °C above the 1850-1900 average, indicating continued warming.

Temperature anomalies were not the same everywhere. Most land and ocean areas were warmer than the 1981-2010 average for the year so far (Figure 3). The period 1981-2010 is used as a baseline for the temperature maps because there are insufficient data in the 19th century in most areas to calculate anomalies relative to a pre-industrial baseline. Areas of unusual warmth during the year included the exceptionally high summer-average temperatures over western Eurasia and parts of east Asia. Colder than average conditions affected Canada, southern Africa, and southern South America with Uruguay recording its coldest January to September since 1988. Cooler than average conditions in the tropical Pacific are associated with the ongoing La Niña as are warmer than average conditions in an area surrounding the La Niña “cold tongue” running from the north Pacific, along the western rim of the Pacific, and down into the south Pacific.

[6] WMO El Niño/La Niña update, August 2022 https://filecloud.wmo.int/share/s/P4xHawHxTlKGmP1YQrb2lQ

[7] Intergovernmental Panel on Climate Change (IPCC), 2021: Summary for Policymakers, A.1.2. In: AR6 Climate Change 2021: The Physical Science Basis, https://www.ipcc.ch/report/ar6/wg1/downloads/report/IPCC_AR6_WGI_SPM_final.pdf. The IPCC average was based on four data sets: HadCRUT5, NOAAGlobalTemp—Interim, Berkeley Earth and Kadow, C.; Hall, D. M.; Ulbrich, U. Artificial Intelligence Reconstructs Missing Climate Information. Nature Geoscience 2020, 13 (6), 408–413. https://doi.org/10.1038/s41561-020-0582-5. Bracketed values indicate the 5%–95% confidence range.

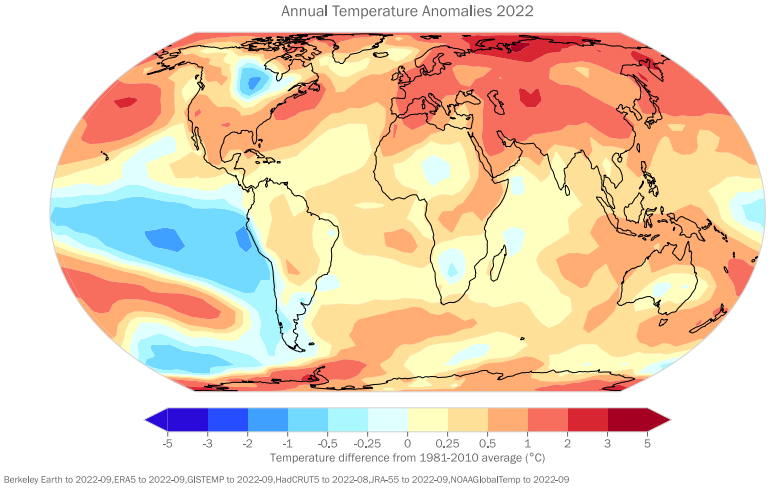

Figure 3: Near-surface temperature differences relative to the 1981–2010 average for 2022 to September. The map shows the median anomaly calculated from six data sets: HadCRUT5, ERA5, JRA-55, GISTEMP, NOAAGlobalTemp and Berkeley Earth.

Ocean heat content

Increasing human emissions of CO_2 and other greenhouse gases cause a positive radiative imbalance at the top of the atmosphere – the Earth energy Imbalance – leading to an accumulation of energy in the form of heat in the Earth system that is driving global warming[8,9,10]. Around 90% of this accumulated heat in the Earth system is stored in the ocean, which is measured through Ocean Heat Content (OHC). A positive Earth energy Imbalance signals that the Earth's climate system is still responding to the current forcing[11] and that more warming will occur even if the forcing does not increase further[12]. The Intergovernmental Panel on Climate Change (IPCC) concluded that "*It is virtually certain that the global upper ocean (0–700 m) has warmed since the 1970s and extremely likely that human influence is the main driver.*"[13,14].

The upper 2000m of the ocean continued to warm in 2021[15] (the latest year for which consolidated figures are available) and it is expected that it will continue to warm in the future – a change which is irreversible on centennial to millennial time scales[16,17]. The ocean heat content in 2021 was the highest on record, exceeding the 2020 value by 14 ± 9 ZJ (Figure 4). All data sets agree that ocean

[8]Hansen, J. et al. (2011). Earth's energy imbalance and implications. Atmospheric Chemistry and Physics https://doi.org/10.5194/acp-11-13421-2011

[9] Rhein, M. et al. 2013. Climate change 2013: The physical science basis.

[10] von Schuckmann, K. et al. (2016). An imperative to monitor Earth's energy imbalance. In Nature Climate Change. https://doi.org/10.1038/nclimate2876

[11] Hansen, J. et al. (2005). Earth's Energy Imbalance: Confirmation and Implications. Science, 308(5727), 1431 LP – 1435. https://doi.org/10.1126/science.1110252

[12] Hansen, J. et al. (2017). Young people's burden: requirement of negative CO2 emissions. Earth Syst. Dynam., 8(3), 577–616. https://doi.org/10.5194/esd-8-577-2017

[13] IPCC, 2021: Summary for Policymakers. In: Climate Change 2021: The Physical Science Basis. Contribution of Working Group I to the Sixth Assessment Report of the Intergovernmental Panel on Climate Change [Masson-Delmotte, V., et al. (eds.)]. Cambridge University Press, Cambridge, United Kingdom and New York, NY, USA, pp. 3−32, doi:10.1017/9781009157896.001. https://www.ipcc.ch/report/ar6/wg1/downloads/report/IPCC_AR6_WGI_SPM.pdf

[14] Cheng, L.; Trenberth, K. E.; Fasullo, J. et al. Improved estimates of ocean heat content from 1960 to 2015, Science Advances 2017, 3 (3), e1601545. https://doi.org/10.1126/sciadv.1601545

[15] von Schuckmann, K., Cheng, L., Palmer, M. D., Hansen, J., Tassone, C., Aich, V., Adusumilli, S., Beltrami, H., Boyer, T., Cuesta-Valero, F. J., Desbruyères, D., Domingues, C., García-García, A., Gentine, P., Gilson, J., Gorfer, M., Haimberger, L., Ishii, M., Johnson, G. C., … Wijffels, S. E. (2020). Heat stored in the Earth system: where does the energy go? Earth Syst. Sci. Data, 12(3), 2013–2041. https://doi.org/10.5194/essd-12-2013-2020

[16] Cheng, L.; Trenberth, K. E.; Fasullo, J. et al. Improved estimates of ocean heat content from 1960 to 2015, Science Advances 2017, 3 (3), e1601545. https://doi.org/10.1126/sciadv.1601545.

[17] IPCC, 2019: Summary for Policymakers. In: IPCC Special Report on the Ocean and Cryosphere in a Changing Climate [H.-O. Pörtner, D.C. Roberts, V. Masson-Delmotte, P. Zhai, M. Tignor, E. Poloczanska, K. Mintenbeck, A. Alegría, M. Nicolai, A. Okem, J. Petzold, B. Rama, N.M. Weyer (eds.)]. In press.

warming rates show a particularly strong increase in the past two decades. The rate of ocean warming for the 0-2000m layer was 0.6 ± 0.1 W·m^{-2} from 1971-2021, but 1.0 ± 0.1 W·m^{-2} from 2006-2021.

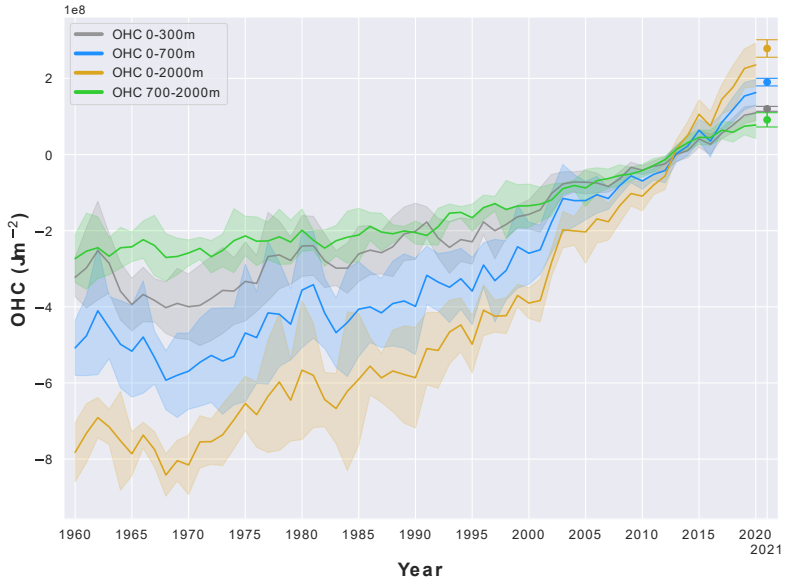

Figure 4: 1960-2021 ensemble mean time series and ensemble standard deviation (2-standard deviations, shaded) of global ocean heat content (OHC) anomalies relative to the 2005-2017 average for the 0-300m (grey), 0-700m (blue), 0-2000m (yellow) and 700-2000m depth layer (green). The ensemble mean is an update of the outcome of a concerted international effort[18], and all products used are referenced in the section on Ocean heat content data. Note that values are given for the ocean surface area between 60°S-60°N and limited to areas deeper than 300m in each product. The ensemble-mean OHC anomalies for the year 2021 has been added as separate points, together with their ensemble spread, and is based on the 4 products listed in Ocean heat content.

Sea level

In 2022, global mean sea level (GMSL) has continued to rise (Figure 5). The GMSL rise is estimated to be 3.4 ± 0.3 mm·yr^{-1} over the 30 years (1993-2022) of the satellite altimeter record, but the rate has doubled between the first decade of the record (1993-2002) and the last (2013-2022) during which the rate has exceeded 4.4 mm·yr^{-1}. The GMSL acceleration is estimated to be 0.12 ± 0.05 mm·yr^{-2} over the 30-year period. GMSL increased by about 5 mm between January 2021 and August 2022. Since January 2020, the increase in GMSL amounts to around 10 mm, a substantial fraction of the GMSL rise since 1993 (around 100 mm), despite the ongoing La Niña.

[18] von Schuckmann, K., Cheng, L., Palmer, M. D., Hansen, J., Tassone, C., Aich, V., Adusumilli, S., Beltrami, H., Boyer, T., Cuesta-Valero, F. J., Desbruyères, D., Domingues, C., García-García, A., Gentine, P., Gilson, J., Gorfer, M., Haimberger, L., Ishii, M., Johnson, G. C., … Wijffels, S. E. (2020). Heat stored in the Earth system: where does the energy go? Earth Syst. Sci. Data, 12(3), 2013–2041. https://doi.org/10.5194/essd-12-2013-2020

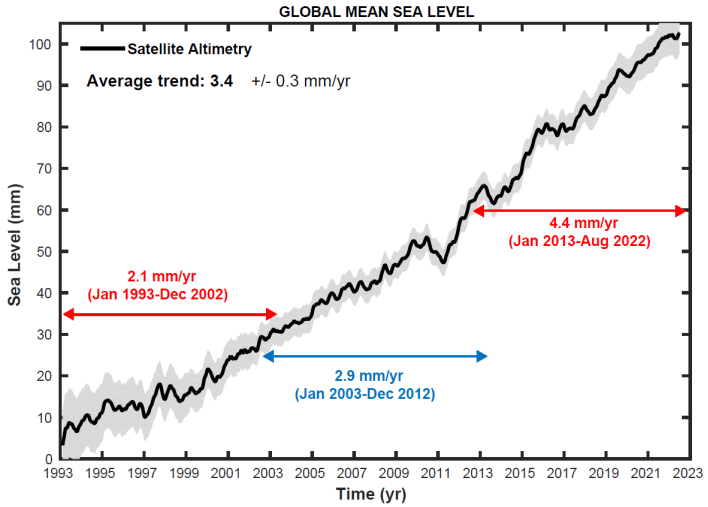

Figure 5: Global mean sea level evolution from January 1993 to August 2022 (black curve) with associated uncertainty (shaded area) The horizontal, coloured straight lines represent the average linear trends over three successive time spans. (Source LEGOS; data from AVISO altimetry www.aviso.altimetry.fr)

Marine heatwaves

As with heatwaves and cold spells on land, marine heatwaves (MHW) and marine cold-spells (MCS) are prolonged periods of extreme heat or cold in the seas and oceans that can have a range of consequences for marine life and dependent communities. MHWs have become more frequent over the 20th and 21st Century while MCS have become less frequent. Satellite retrievals of sea-surface temperature are used to monitor MHWs and MCSs globally, categorised here as *moderate*, *strong*, *severe*, or *extreme* (for definitions, see Data sets and methods).

Overall, 55% of the ocean surface experienced at least one MHW during 2022 (Figure 6) – less than the record of 65% in 2016 and the lowest annual coverage since 2012 (57%). In total, 22% of the ocean surface experienced at least one MCS during 2022 (Figure 7), less than 2021 (25%), and much less than the 1985 record (63%).

The ongoing La Niña and associated lower-than-average sea-surface temperatures mean that the equatorial Pacific is one of the few ocean regions to see wide-spread coverage of *strong* MCS in 2022 (Figure 7). The Southern Ocean is, however, the only region in which MCSs have seen a long-term increase in duration. In the Arctic, the Laptev and Beaufort Seas experienced *severe* and *extreme* MHWs from northern hemisphere spring to autumn of 2022. The ice-edge to the north of Svalbard and east of the Ross Sea experienced notable *extreme* MHW for the second consecutive year.

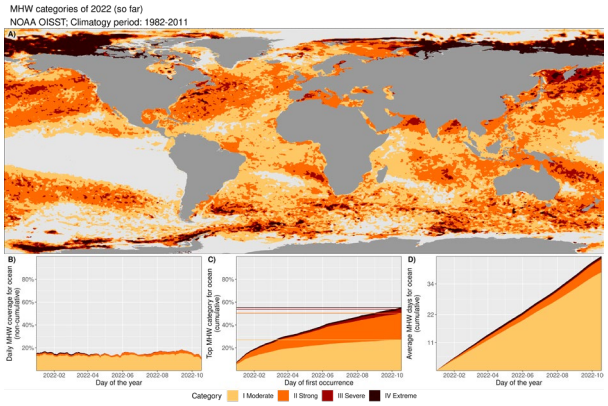

Figure 6: (a) Global map showing the highest MHW category (for definitions, see Marine heatwave and marine cold-spell data) experienced at each pixel over 2022 to 17 October (reference period 1982–2011). Light grey indicates that no MHW

occurred in a pixel over the entire year; (b) Stacked bar plot showing the percentage of the surface of the ocean experiencing an MHW on any given day of the year; (c) Stacked bar plot showing the cumulative percentage of the surface of the ocean that experienced an MHW over the year. Note: These values are based on when in the year a pixel first experienced its highest MHW category, so no pixel is counted twice. Horizontal lines in this figure show the final percentages for each category of MHW; d) Stacked bar plot showing the cumulative number of MHW days averaged over the surface of the ocean. Note: This average is calculated by dividing the cumulative sum of MHW days per pixel weighted by the surface area of those pixels. Data are from NOAA OISST. Source: Robert Schlegel

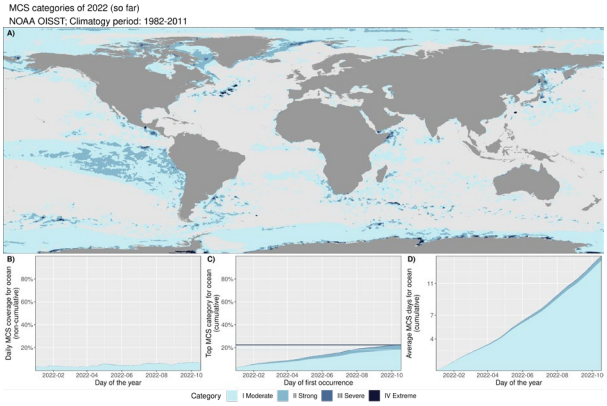

Figure 7: as for Figure 6 but showing marine cold-spells (MCSs) rather than marine heatwaves (MHWs). Data are from NOAA OISST. Source: Robert Schlegel

Cryosphere

The cryosphere comprises the frozen parts of the earth – glaciers and ice sheets, sea ice, snow, and permafrost. Satellites provide long-term measurements of many aspects of the cryosphere, providing a complementary source of information to the data gathered in situ in the remote and often inhospitable environments in which the components of the cryosphere are found.

Sea ice

Arctic sea-ice extent was below the long-term (1981-2010) average for most of the year, with a Spring sea-ice maximum of 14.59 million km^2 in March 2022, 0.84 million km^2 below the long-term mean (Figure 8). The September extent was 4.87 million km^2, 1.54 million km^2 below the long-term mean extent. This represents greater ice extent than the average minimum values of the last decade – a moderate summer for Arctic sea-ice melt – but it is tied for the 11th lowest monthly minimum ice extent in the satellite record. The smallest daily extent of the year, 4.67 million km^2, occurred around 18 September and was the 9th or 10th lowest annual-minimum daily extent on record[19,20].

Sea ice extent in the Antarctic has seen both record high (2014) and low (2017/2022) extents in the past 10 years (Figure 8). Antarctic sea-ice extent dropped to 1.92 million km^2 on February 25 2022, the lowest level on record and almost 1 million km^2 below the long-term (1981-2010) mean[21]. The origins of the ice loss can be traced back to October/November 2021 when there was a series of very deep storms to the west of the Antarctic Peninsula. This area is strongly influenced by the phase of the El Niño – Southern Oscillation and the deep storms in late 2021 were consistent with the La Niña conditions at the time.

Following the annual sea ice extent minimum in February, the total extent of Antarctic sea ice has been continuously below the 30-year (1981-2010) mean up to October 2022; it was even record low at times in June and July. The Weddell Sea, Indian Ocean and Pacific sectors have all retained negative

[19] https://climate.copernicus.eu/sea-ice-cover-september-2022
[20] https://nsidc.org/arcticseaicenews/2022/09/arctic-sea-ice-minimum-ties-tenth-lowest/
[21] Turner, J., Holmes, C., Caton Harrison, T., Phillips, T., Jena, B., Reeves-Francois, T., et al. (2022). Record low Antarctic sea ice cover in February 2022. Geophysical Research Letters, 49, e2022GL098904. https://doi.org/10.1029/2022GL098904

sea ice extent anomalies since February 2022, leading to the total Southern Ocean ice extent being about 0.5 million km^2 below the mean maximum extent in October 2022.

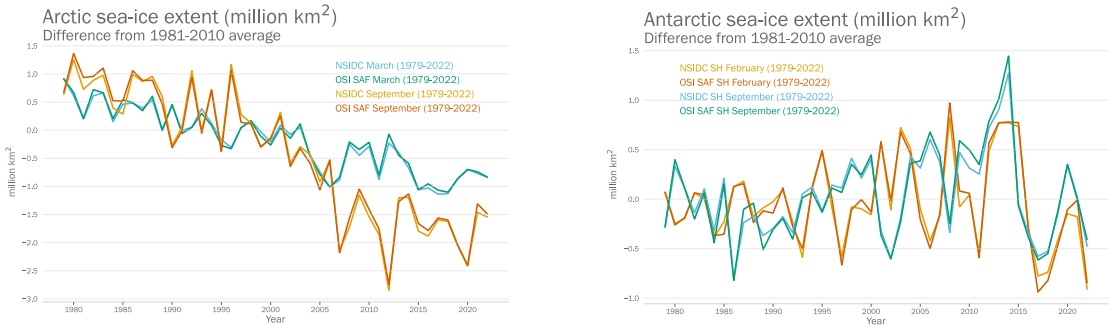

Figure 8: Sea ice extent anomalies (relative to the 1981-2010 average) from 1979 to 2022 for (left) the Arctic and (right) the Antarctic. Blue/green lines indicate the anomalies in annual maximum ice extent (March for the Arctic and September for the Antarctic) and orange/red correspond to the annual minimum ice extent (September for the Arctic and February for the Antarctic). Data from EUMETSAT OSI SAF v2p1 and National Snow and Ice Data Centre (NSIDC) v3 (Fetterer et al., 2017) (see details in Sea ice).

Glaciers

Glaciers are formed from snow that has compacted to form ice, which deforms and flows downhill to lower and warmer altitudes, where it melts. Where glaciers terminate in a lake or the ocean, ablation also occurs through melting at the ice-water interface and through calving processes.

According to the World Glacier Monitoring Service, in the hydrological year 2020-2021, the 40 or so glaciers with long-term observations experienced an average mass balance of –0.77 m water equivalent (m w.e.). This is a smaller loss than the average for the last decade but still more than the average for the period 1991-2020. Preliminary results for 2022 are only available for a few selected regions at this time, as field observations are recently completed and need to be evaluated. We report here on preliminary data from the Swiss Alps.

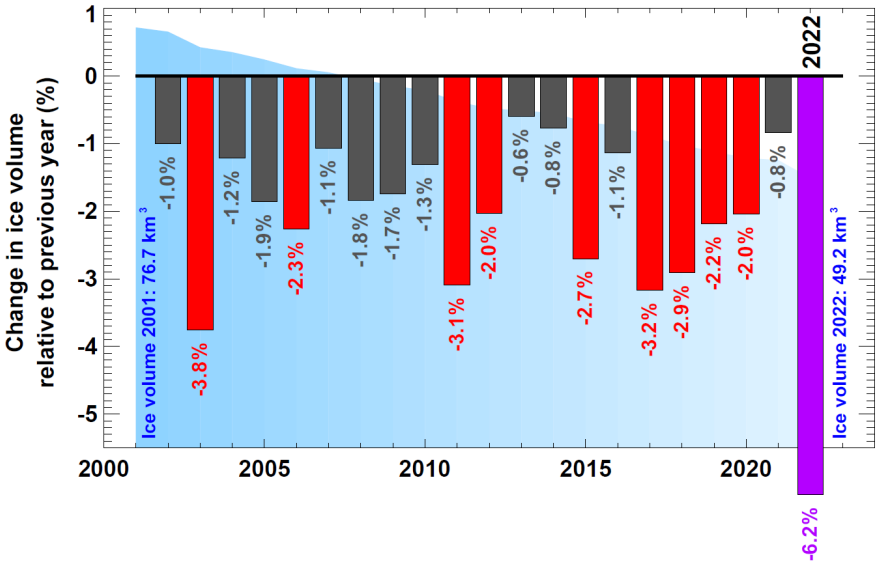

Figure 9: Total annual loss of Swiss glaciers related to the current ice volume 2002-2022. The vertical bars indicate the percentage change in ice volume relative to the previous year. Red bars are the 10 largest relative mass losses on record. The purple bar is the relative mass loss for 2022. The blue shaded area in the background represents the overall ice volume.

In the European Alps, records of glacier mass loss were shattered in 2022. Mass losses were far beyond the range of historical variability. Average thickness changes of between 3 and over 4 metres were

measured throughout the Alps, substantially more than in the previous record year 2003. In Switzerland 6% of the glacier ice volume was lost between 2021 and 2022 (Figure 9). There are three reasons for this extreme glacier melt. First, there was very little winter snow and this meant that the ice was unprotected in early summer. Second, Saharan dust blew over the Alps darkening the snow surface, thus further accelerating melt. Third, long and persistent heat waves between May and early September 2022 led to massive ice loss. For the first time in history, no snow outlasted the summer season even at the very highest measurement sites and thus no accumulation of fresh ice occurred. Between 2001 and 2022 the volume of glacier ice in Switzerland decreased from 77 km^3 to 49 km^3, a decline of more than a third.

Greenland ice sheet

An ice sheet is an area of glacial ice that exceeds 50 000 km^2. In the current climate there are two ice sheets: one on Greenland, the other on Antarctica.

The total mass balance of the Greenland ice sheet is the sum of three components: the surface mass balance, the marine mass balance and the basal mass balance. The surface mass balance is the difference between snow accumulation and meltwater runoff from the ice sheet. The marine mass balance is the mass loss at the edge of the ice sheet from the calving of icebergs and the melting of glacier tongues in contact with the ocean. Basal mass balance consists of melting at the ice sheet bed.

For Greenland[22] the estimated total mass balance[23] was -85 Gt representing a net ice loss during the 2022 mass balance year (1 September 2021 – 31 August 2022). This year, the Greenland ice sheet ended with a surface mass balance of about 423 Gt, which is the 10th highest value in the dataset that goes back 1980 (Figure 10 left). Nevertheless, the Greenland Ice Sheet ended with a negative total mass balance for the 26th year in a row, mainly due to the strong negative marine mass balance of -486 Gt.

The melting and ablation seasons in Greenland began late in 2022 and the summer was relatively cool compared with recent years. However, there was a period of high temperatures at the end of July 2022 with intense surface melt over large parts of the ice sheet and large ice losses over a few days. September 2022 was also extraordinarily warm, with widespread and generally high positive temperature anomalies along with widespread melting early in the month (Figure 10 right). Summit Station, the highest point in Greenland (3 200 m), had its warmest September on record (since 1991) and experienced melting conditions on September 3, 2022, the first time melting has been registered at this site in September[24]. Later in September, heavy rain associated with post-tropical cyclone Fiona fell on the ice sheet, also a first for September.

[22] Based on the average of three regional climate and mass balance models. See Mankoff, K. D., X. Fettweis, P.L. Langen, M. Stendel, K.K. Kjeldsen, N.B. Karlsson, B. Noël, M.R. van den Broeke, W. Colgan, S.B. Simonsen, J.E. Box, A. Solgaard, A.P. Ahlstrøm, S.B. Andersen and R.S. Fausto, 2021: Greenland ice sheet mass balance from 1840 through next week. Earth Syst. Sci. Data 13, 5001–5025, doi: 10.5194/essd-13-5001-2021

[23] A negative mass balance indicates a loss of ice mass, a positive mass balance indicates a gain.

[24] https://nsidc.org/greenland-today/

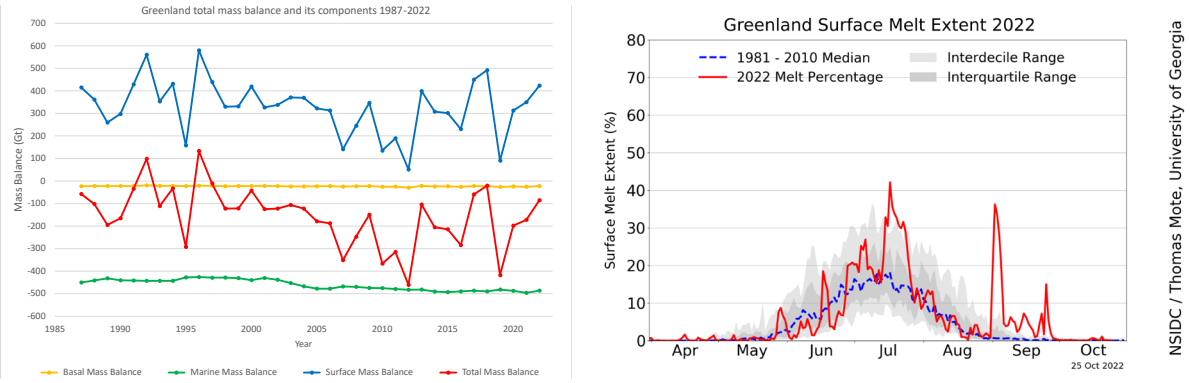

Figure 10: (left) Components of the total mass balance of the Greenland Ice Sheet 1987-2022. Blue: Surface mass balance (SMB), green: marine mass balance (MMB), orange: basal mass balance (BMB), red: total mass balance (TMB), the sum of SMB, MMB and BMB. Mankoff et al. (2021), updated and redrawn by M. Stendel. (right) Greenland Ice Sheet melt extent, 2022.. Image and analysis courtesy of Thomas Mote, U.S. National Snow and Ice Data Center.

Precipitation

Precipitation totals were above the long-term average (Figure 11) in northeast Asia, the western Indian summer monsoon region, southeast Asia, the Maritime Continent, Australia, New Zealand, areas of northern South America, parts of North America and the Caribbean, west Africa, Sudan, coastal areas extending from western Libya to Egypt, and the southern Arabian Peninsula including UAE, Oman and Yemen.

Regions with a marked rainfall deficit included: Europe, Central Asia, Northern Australia, Eastern Africa, most of North Africa, central and southern South America, and central and western North America. The Indian Monsoon onset was earlier and the withdrawal later than normal this year. The majority of the Indian Subcontinent received high precipitation totals and the monsoon extended farther westward then usual towards Pakistan where there was extensive flooding.

La Niña brings distinctive patterns of rainfall, which are described in the next section, Short-term climate drivers.

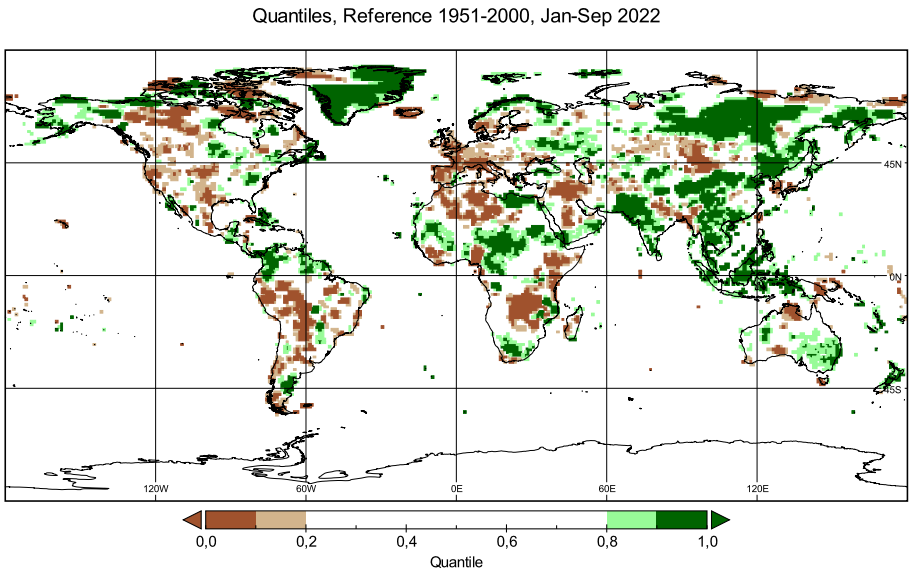

Figure 11: Total precipitation in Jan-Sep 2022, expressed as a percentile of the 1951–2000 reference period, for areas that would have been in the driest 20% (brown) and wettest 20% (green) of years during the reference period, with darker shades of brown and green indicating the driest and wettest 10%, respectively (Source: Global Precipitation Climatology Centre (GPCC), Deutscher Wetterdienst, Germany)

Short-term climate drivers

There are many different natural phenomena, often referred to as climate patterns or climate modes, that affect weather at timescales ranging from days to several months or even years. In 2022, the El Niño–Southern Oscillation (ENSO) and the Indian Ocean dipole (IOD) contributed to major weather and climate events across large areas of the world.

ENSO – El Niño Southern Oscillation

ENSO is one of the most important drivers of year-to-year variability in weather patterns worldwide. It is linked to hazards such as heavy rains, floods, and drought. El Niño, characterised by higher-than-average sea surface temperatures in the eastern tropical Pacific and a weakening of the trade winds, typically has a warming influence on global temperatures. La Niña, which is characterised by below-average sea surface temperatures in the central and eastern tropical Pacific and a strengthening of the trade winds, has the opposite effect.

La Niña conditions emerged in mid-2020 and continued into 2021 with sea surface temperatures briefly becoming ENSO-neutral (temperatures within 0.5 °C of normal, Figure 12), although still cooler than average during most of the Northern Hemisphere summer. Temperatures declined again, and La Niña re-emerged during the July−September period of 2021, quickly evolving to a moderate strength event where it remained through at least September 2022. Indications are that La Niña is likely to continue through northern hemisphere autumn, which would mark the third consecutive year of La Niña[25]. This is the third time such an event has occurred in the last 50 years, following 1973-76 and 1998-2001.

As well as having a temporary cooling influence on global temperature, La Niña is often – though not always – associated with characteristic patterns of rainfall. In some regions the pattern of precipitation anomalies in 2022 was typical of La Niña: drier than usual conditions in Patagonia and southwest North America, and wetter than usual in Southern Africa, northern South America, the maritime continent and eastern Australia.

More intense and longer monsoon rainfall in southeast Asia is associated with La Niña. Pakistan experienced heavy rains in July and August. La Niña is also associated with drier-than-normal conditions in east Africa. Most of Kenya, Ethiopia, and Somalia have experienced four consecutive below-average rainfall seasons with severe humanitarian impacts[26]. More details are to be found in the section on Selected high impact events.

Although it typically reduces global temperature, La Niña is not associated with lower temperatures everywhere. In New Zealand it is typically associated with warm and wet air masses. The country reported its fifth warmest summer (2020/21), followed by its second warmest autumn and its warmest and wettest winter on record. This marked the third consecutive winter to break the temperature record.

[25] WMO ENSO update https://public.wmo.int/en/our-mandate/climate/el-ni%C3%B1ola-ni%C3%B1a-update
[26] https://reliefweb.int/report/ethiopia/horn-africa-drought-regional-humanitarian-overview-call-action-revised-24-august-2022

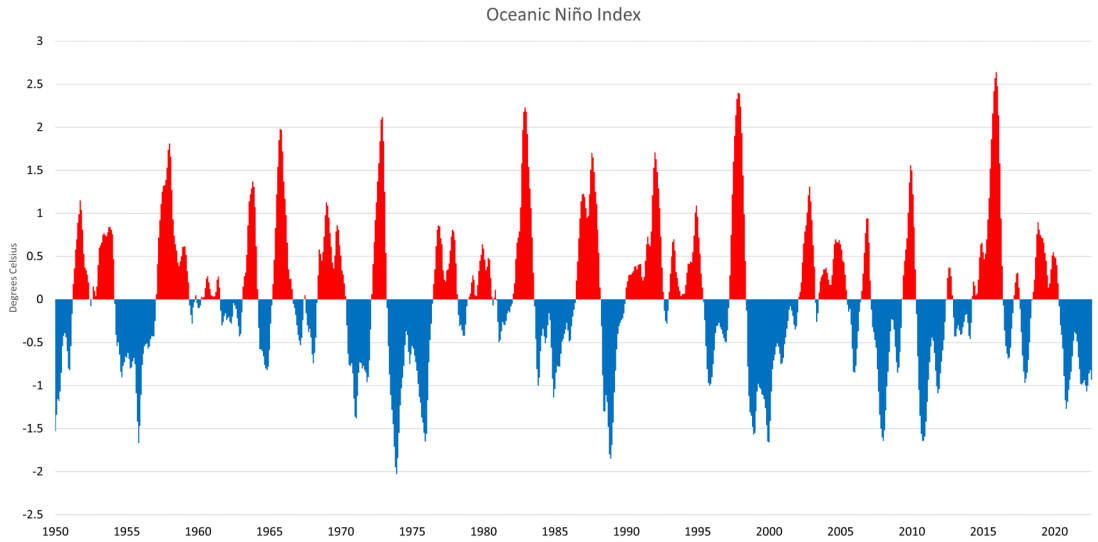

Figure 12: Time series of NOAA's Oceanic Niño index from 1950 to August 2022 showing the presence of below-average conditions (blue) and above average conditions (red) during 3-month average time periods. (Source: NOAA NCEI)

IOD – Indian Ocean Dipole

The positive phase of the IOD is characterised by below-average sea-surface temperatures in the eastern Indian Ocean and above average sea-surface temperatures in the west. The negative phase has the opposite pattern. The resulting change in the gradient of sea-surface temperature across the ocean basin affects the weather of the surrounding continents, primarily in the Southern Hemisphere. Positive IOD events are often associated with El Niño and negative events with La Niña.

For the second consecutive year, a negative IOD developed during austral winter. In combination with La Niña, this phase contributed to wet conditions across much of Australia in late austral winter and spring. It was the wettest winter since 2016 for both Queensland and the Northern Territory. Conversely, the negative IOD, again in combination with La Niña, is contributing once again to the extreme dry conditions in eastern Africa.

Selected high impact events

Although the broad-scale changes in the climate, as tracked by the key indicators, are important, the impacts of weather and climate are most often and most clearly felt during extreme events such as heavy rain and snow, droughts, heatwaves, cold waves and storms, including tropical storms and cyclones. In conjunction with other factors, these can lead to or exacerbate other high-impact events such as flooding, landslides, and wildfires.

This section, describes a small selection of high-impact events of 2022 and is based on input from WMO Members and UN agencies. This represents only a small selection of the events of 2022 and a wider range of extreme events and their impacts will be shared via the StoryMap.

South Asia heatwaves and floods

The pre-monsoon period was exceptionally hot in India and Pakistan. Pakistan had its hottest March and hottest April on record. The heat caused a decline in crop yields. This combined with the banning of wheat exports and restrictions on rice exports in India are threatening the international food markets and posing risks to countries already affected by shortages of staple foods[27].

[27] BMJ. 2022;378 :e071534 http://dx.doi.org/10.1136/bmj-2022-071534 Published: 29 September 2022

Pakistan experienced exceptional flooding during the monsoon season, peaking in late August. July (181% above normal) and August (243% above normal) were each the wettest on record nationally. Sindh province was particularly badly affected, with Balochistan also hard-hit. Preliminary satellite data indicated that 75 000 square kilometres, about 9% of Pakistan's area, was inundated at some stage during August[28]. 1 700 people died[29] in the floods along with 936 000 head of livestock. Rainfall-triggered flooding and landslides have also substantially disrupted transportation and building infrastructure, and food prices increased by 29%[30]. Some 33 million people were affected, and 7.9 million people were displaced, with nearly 600 000 living in relief sites[31]. The flooding in Pakistan led to the spread of water-borne diseases with the greatest impacts among the most vulnerable and food-insecure regions of southern and central Pakistan. As it could take months for the water to recede, the threat of waterborne diseases and food inaccessibility are expected to rise.

Adjacent areas of Afghanistan were also affected. There was also significant flooding in India at various stages during the monsoon season, particularly in the north-east in June, with over 700 deaths reported during the season from flooding and landslides, and a further 900 from lightning. Floods also triggered 663 000 displacements in the Indian state of Assam[32].

In Bangladesh, the worst floods in 20 years have affected some 7.2 million people with 481 000 displacements recorded[33]. In Cox's Bazar, heavy rains affected nearly 60 000 refugees and triggered secondary displacement[34]. Emergency shelter assistance was provided to over 15 000 affected families[35].

Drought in the Greater Horn of Africa

Drought intensified in the Greater Horn of Africa region, focused on Kenya, Somalia, and southern Ethiopia. Rainfall was well below average across the region in the March-May rainy season, the fourth consecutive poor wet season since the second half of 2020, which was the longest such sequence in 40 years. As in the previous prolonged drought in 2010-12, La Niña and the negative Indian Ocean Dipole were substantial contributors to the dry conditions. The seasonal forecasts for the October-December 2022 rains indicate yet another below-average season, which will likely result in crop failure and further exacerbate the food insecurity situations in Kenya, Somalia, and Ethiopia.

Across the East Africa region, under the effects of the drought and other shocks, an estimated 18.4 to 19.3 million people have faced food Crisis or worse levels of acute food insecurity before June 2022[36]. Paired with funding shortfalls and the global increase in food prices, more than 3.5 million refugees in the region (75% of the total refugee population) have been affected by major cuts in food assistance[37]. Over 1.1 million people have been internally displaced in Somalia as a consequence of the drought by September 2022[38]. Fleeing a complex mix of conflict and drought, over 16 000 Somali refugees arrived

[28] https://www.unitar.org/maps/map/3604
[29] NDMA Monsoon 2022 Daily Situation Report No 115 (Dated 6th Oct, 2022) https://reliefweb.int/report/pakistan/ndma-monsoon-2022-daily-situation-report-no-115-dated-6th-oct-2022 (Dated 20th Oct, 2022) https://reliefweb.int/report/pakistan/ndma-monsoon-2022-daily-situation-report-no-129-dated-20th-oct-2022
[30] WFP and FAO. 2022. Hunger Hotspots. FAO-WFP early warnings on acute food insecurity: June to September 2022 Outlook. Rome. https://www.wfp.org/publications/hunger-hotspots-fao-wfp-early-warnings-acute-food-insecurity-june-september-2022
[31] UNHCR News- UNHCR urgently seeks US$66 million for communities devastated by Pakistan floods | October 2022; IOM: Pakistan Floods Response Situation Report. September 2022.
[32] IDMC mid-year update | September 2022
[33] IDMC mid-year update | September 2022
[34] ISCG Flash Update #6 on Monsoon Response of 25 August 2022
[35] ISCG Flash Update #6 on Monsoon Response of 25 August 2022
[36] International Bank for Reconstruction and Development / The World Bank 2022. Food Security update, September 29, 2022.
[37] UNHCR East and Horn of Africa, and the Great Lakes Region Operational Update Region | April - June 2022
[38] OCHA, UNHCR, IOM Somalia: Drought and Famine Displacement Monitoring Dashboard (September 2022)

in Dollo Ado, Ethiopia and another 10 000 in Kenya until June 2022[39]. Adding to the multiple risks already faced by displaced people, resilience to climate-related disasters, environmental degradation and displacement is often lowest in conflict-affected contexts.

Southern Africa floods

Many of the high-impact disasters in 2022 happened consecutively, leaving little time for recovery between one shock and the next. The southern Africa region has been battered by a series of cyclones over two months, leading to a surge in the need for protection and shelter for hundreds of thousands of affected persons, including refugees and Internally Displaced Persons (IDPs) [40].

Madagascar had four landfalls in the space of a month in late January and February. Ana (January) and Batsirai (February) both caused significant loss of life there, with Ana also going on to have major impacts from flooding in Mozambique and Malawi. Gombe (March) brought flooding to Mozambique with significant casualties.

More than 190 000 people who lost or fled their homes during Tropical Storm Ana in January remained displaced inside Malawi in April[41]. Two months after the storm had displaced over 20 000 IDP households in Mozambique[42], UNHCR recorded 736 000 people affected by Tropical Cyclone Gombe in Nampula and Zambezia provinces, while over 129 000 people were internally displaced[43].

Subtropical Depression Issa, in combination with a cut-off low pressure system, caused extreme flooding in April in the KwaZulu-Natal region of eastern South Africa, with rainfall totals of up to 311 mm in 24 hours on 11-12 April. Over 400 deaths were attributed to the flooding, which also displaced 40 000 people, with direct impacts on transportation, buildings, and water infrastructure, thus affecting post-harvest facilities for agrifood storage and processing, transportation, markets and consumption through reduced access to facilities and reduced income[44].

The south and western regions of Madagascar entered an extended multi-year dry period since 2015-16 during which there have been droughts of varying severity nearly every season. Whilst significant rain fell during 2021-22 in many parts of southern Africa, long-term localised drought persists in some areas, especially in southern Madagascar, where rainfall totals have been below average in most years since 2011.

Northern hemisphere summer heatwaves and drought

Exceptionally hot and, in places, dry conditions affected China, Europe and North Africa during the summer.

China had the most extensive and long-lasting heatwave since national records began, extending from mid-June to the end of August and resulting in the hottest summer on record by a margin of more than 0.5 °C. It was also the second-driest summer on record, with most of the southern half of China (apart from Guangdong province) having seasonal rainfall 20% to 50% below average. The heat was particularly severe in the Yangtze River valley, which also suffered from significant drought during its driest summer on record; the Yangtze River at Wuhan reached its lowest recorded level for August. There were also numerous wildfires in the region.

[39] East and Horn of Africa, and the Great Lakes Region: UNHCR Drought Situation Response Update #1 | August 2022
[40] UNHCR News- Urgent help needed in Malawi to rebuild lives wrecked by Tropical Storm Ana | April 2022
[41] UNHCR News- Urgent help needed in Malawi to rebuild lives wrecked by Tropical Storm Ana | April 2022
[42] IOM Mozambique – Tropical Storm Ana Flash Report 03 (02 February 2022)
[43] UNHCR Mozambique Country Factsheet | August 2022; IOM Displacement Tracking Mechanism, Round 16, June 2022..
[44] BMJ. 2022;378: e071534 http://dx.doi.org/10.1136/bmj-2022-071534 Published: 29 September 2022

Europe also experienced numerous major heatwaves during the summer, with significant heatwaves occurring in each of the three summer months. The most exceptional occurred in mid-July. The temperature exceeded 40 °C in the United Kingdom for the first time, with a reading of 40.3 °C at Coningsby on 19 July[45], 1.6 °C above the previous national record, whilst 33.0 °C on 18 July at Phoenix Park (Dublin) was the highest in Ireland since 1887. Numerous locations broke previous records by more than 3 °C, particularly in northern England and western France. The heat extended as far north as Sweden, where 37.2 °C at Målilla on 21 July was the country's highest since 1947. South-western France was particularly affected by wildfires, with over 62 000 hectares burnt, whilst there was significant property loss in several fires in the outer suburbs of London. In Portugal, the hydrological year (October-September) was the third driest on record and the summer heat exacerbated the already severe drought situation[46,47]. These conditions fuelled severe wildfires and the total burned area in 2022 (to 15 October) was 110 000 ha, the highest since the catastrophic fire season of 2017[48].

The Mediterranean region experienced major heatwaves in June and August. Tunisia had its hottest June on record and some locations set record highs in August. For the second consecutive year, wildfires caused major loss of life in Algeria, with 44 deaths reported in fires from 16 to 18 August.

Estimated mortality due to the heat is complicated by changes in background death rates due to COVID. Nevertheless, some official estimates have been made including around 2 800 deaths in the UK[49] (among those aged 65 and older), 4 500 in Germany[50], and 11 000 in France[51].

Drought also affected many parts of Europe and the Mediterranean. In Europe, conditions were at their most severe in August, when rivers including the Rhine, Loire and Danube fell to critically low levels. Three states in west-central Germany had their driest summer on record. France had its driest January to September period since 1976, and the United Kingdom and Uccle (Belgium) had their driest January to August since 1976, while the 12 months ending in August 2022 were the driest for at least 40 years in Morocco. Significant drought also continues to affect parts of southwest Asia, particularly Iran and Iraq.

Hurricane Ian

In late September, Hurricane Ian formed in the western Caribbean[52]. On September 27, Hurricane Ian crossed western Cuba before intensifying to category 4 and making landfall in southwest Florida on 28 September, bringing extensive storm-surge inundation in low-lying coastal areas and river flooding further northeast, where 4-day rainfalls exceeded 500 mm in the Daytona Beach area. Ian made landfall with sustained 10-minute winds of 241 km/h (150 mph), the fourth-strongest landfall on record in Florida. 131 deaths were reported in the US with additional loss of life in Cuba[53].

[45] https://www.metoffice.gov.uk/about-us/press-office/news/weather-and-climate/2022/july-heat-review
[46] IPMA: https://www.ipma.pt/resources.www/docs/im.publicacoes/edicoes.online/20221007/aiheZPiRtGVzsVeKFTuO/cli_20220901_20220930_sec_mm_co_pt.pdf
[47] IPMA: https://www.ipma.pt/pt/oclima/observatorio.secas/
[48] ICNF: https://www.icnf.pt/florestas/gfr/gfrgestaoinformacao/grfrelatorios/areasardidaseocorrencias
[49] https://www.ons.gov.uk/peoplepopulationandcommunity/birthsdeathsandmarriages/deaths/articles/excessmortalityduringheatperiods/englandandwales1juneto31august2022
[50] https://www.rki.de/DE/Content/Infekt/EpidBull/Archiv/2022/42/Art_01.html
[51] From the French contribution
[52] https://www.ncei.noaa.gov/access/monitoring/monthly-report/national/202209/supplemental/page-5
[53] https://www.ncei.noaa.gov/access/billions/events/US/2022

Contributors

Individuals (in alphabetical order)

Signe Aaboe (Norwegian Meteorological Institute), Ahmat Younous Abdel-lathif (WFP), Jorge Alvar-Beltrán (FAO), Jose Álvaro Mendes Pimpao Alves Silva (WMO), Omar Baddour (WMO), Hamza Benlarabi (IOM), Jana Birner (UNHCR), Jessica Blunden (NOAA NCEI), Rogerio Bonifacio (WFP), Tim Boyer (NOAA's National Centers for Environmental Information, Silver Spring, Maryland, USA), Anny Cazenave (LEGOS CNES and OMP), Xuan Che (UNDRR), Lijing Cheng (Institute of Atmospheric Physics, Chinese Academy of Sciences, Beijing, China; Center for Ocean Mega-Science, Chinese Academy of Sciences, Qingdao, 266071, China), John Church (University of New South Wales, Sydney, Australia), Damien Desbruyeres (Ifremer, University of Brest, CNRS, IRD, Laboratoire d'Océanographie Physique et Spatiale, Brest, France), Catia M. Domingues (NOC), Robert Dunn (Met Office, UK) Arianna Gialletti (FAO), Donata Giglio (University of Colorado, Boulder, USA), John E. Gilson (SCRIPPS Institution of Oceanography, University of California San Diego, La Jolla, California, USA), Atsushi Goto (WMO), Yvan Gouzenes (LEGOS and OMP), Stephan Gruber (Carleton University, Ottawa, Canada), Flora Gues (CELAD, Mercator Ocean International, Toulouse, France), Shigeki Hosoda (Japan Marine-Earth Science and Technology (JAMSTEC), Japan), Sander Houweling (Vrije Universiteit Amsterdam, the Netherlands), Matthias Huss (ETH Zürich, Switzerland), Kirsten Isensee (IOC UNESCO), Gregory C. Johnson (NOAA PMEL), Maarten Kappelle (UNEP, Nairobi), John Kennedy (WMO), Rachel Killick (Met Office, UK), Brian King (NOC), Nicolas Kolodziejczyk (University of Brest, CNRS, IRD, Ifremer, Laboratoire d'Océanographie Physique et Spatiale, IUEM, Brest, France), Animesh Kumar (UNDRR), Mikael Kuusela (Carnegie Mellon University, Pittsburg, USA), Thomas Lavergne (Norwegian Meteorological Institute), Yuehua Li (School of Earth Sciences,Yunnan University, Kunming, China), John Lyman (NOAA PMEL), Shawn Marshall (ECCC and University of Calgary), Jesse Mason (WFP), Trevor McDougall (University of New South Wales), Brian Menounos (University of Northern British Columbia, Canada), Audrey Minère (Mercator Ocean International, France), Colin Morice (Met Office, UK), Didier Paolo Monselesan (CSIRO Oceans and Atmosphere), Lev Neretin (FAO), Jeannette Noetzli (Institute for Snow and Avalanche Research, Switzerland), Inès Otosaka (CPOM), Giancarlo Pini (WFP), Claire Ransom (WMO), Dean Roemmich (SCRIPPS Institution of Oceanography, University of California San Diego, La Jolla, California, USA), Kanako Sato (Japan Marine-Earth Science and Technology (JAMSTEC), Japan), Katsunari Sato (Japan Meteorological Agency, Japan), Abhishek Savita (GEOMAR, Kiel, Germany), Yousuke Sawa (Japan Meteorological Agency, WDCGG, Japan), Robert W. Schlegel (Sorbonne Université, CNRS, Laboratoire d'Océanographie de Villefranche), Katherina Schoo (IOC UNESCO), Karina von Schuckmann (Mercator Ocean International), Rahul Sengupta (UNDRR), Martin Stendel (DMI), Dmitry Streletskiy (George Washington University, Washington DC, USA), Toshio Suga (Tohoku University / Japan Marine-Earth Science and Technology (JAMSTEC), Japan), Tanguy Szekely (Ocean Scope, Brest, France), Oksana Tarasova (WMO), Blair Trewin (Bureau of Meteorology), John Turner (BAS), Freja Vamborg (ECMWF), Alex Vermeulen (Carbon Portal, Lund University, Sweden), Ying Wang (UNEP, Nairobi), Susan E. Wjiffels (CSIRO Oceans and Atmosphere, Hobart, Tasmania, Australia Woods Hole Oceanographic Institution, Massachusetts, USA), Markus Ziese (GPCC, DWD, Germany)

WMO Members

Argentina, Australia, Bahrain, Bangladesh, Barbados, Belgium, Bosnia and Herzegovina, Brazil, British Caribbean Territories, Bulgaria, Canada, Cayman Islands, Chile, China, Colombia, Cote d'Ivoire, Croatia, Czech Republic, Denmark, Dominican Republic, Ecuador, Egypt, Estonia, Finland, France, Georgia, Germany, Greece, Grenada, Guatemala, Hungary, Hong Kong (China), India, Indonesia, Iran, Iraq, Ireland, Italy, Japan, Jordan, Kenya, Latvia, Libya, Luxembourg, Macao (China), Madagascar, Maldives, Mali, Mauritius, Morocco, Myanmar, Namibia, New Zealand, North Macedonia, Norway, Pakistan,

Peru, Poland, Russian Federation, Rwanda, Saudi Arabia, Seychelles, Slovakia, Slovenia, South Africa, Sri Lanka, Sweden, Switzerland, Tanzania, Thailand, Trinidad and Tobago, Tunisia, Türkiye, Uganda, Ukraine, United Kingdom, United States, Uruguay, Uzbekistan

UN agencies

United Nations Environment Programme (UNEP), Intergovernmental Oceanographic Commission – United Nations (IOC-UNESCO), United Nations High Commissioner for Refugees (UNHCR), International Organization for Migration (IOM), Food and Agriculture Organization of the United Nations (FAO), World Food Programme (WFP), United Nations Office for Disaster Risk Reduction (UNDRR)

Institutions

British Antarctic Survey (BAS); Bureau of Meteorology; Carbon Portal, Lund University, Sweden; Carleton University, Ottawa, Canada; Carnegie Mellon University, Pittsburg, USA; CELAD, Mercator Ocean International, Toulouse, France; Center for Ocean Mega-Science, Chinese Academy of Sciences, Qingdao, 266071, China; Centre for Polar Observation and Modelling, University of Leeds, UK (CPOM); CSIRO Oceans and Atmosphere, Hobart, Tasmania, Australia; Danmarks Meteorologiske Institut (DMI); Deutscher Wetterdienst (DWD); Environment and Climate Change Canada (ECCC); ETH Zürich, Switzerland; European Centre for Medium-range Weather Forecasts (ECMWF); George Washington University, Washington DC, USA; Global Precipitation Climatology Centre (GPCC); Ifremer, University of Brest, CNRS, IRD, Laboratoire d'Océanographie Physique et Spatiale, Brest, France; Institute for Snow and Avalanche Research, Switzerland; Institute of Atmospheric Physics, Chinese Academy of Sciences, Beijing, China; Japan Marine-Earth Science and Technology (JAMSTEC), Japan; Japan Meteorological Agency, WDCGG, Japan; LEGOS CNES; Mercator Ocean International, Toulouse, France; Met Office, UK; National Oceanographic and Atmosphere Administration, National Centers for Environmental Information (NOAA NCEI); NOAA, Pacific Marine Environmental Laboratory, Seattle, USA (NOAA PMEL); National Oceanographic Centre, Southampton, UK (NOC); Norwegian Meteorological Institute; Ocean Scope, Brest, France; OMP; School of Earth Sciences,Yunnan University, Kunming, China; SCRIPPS Institution of Oceanography, University of California San Diego, La Jolla, California, USA; Sorbonne Université, CNRS, Laboratoire d'Océanographie de Villefranche; Tohoku University, Japan; University of Calgary; University of Colorado, Boulder, USA; University of New South Wales, Sydney, Australia; University of Northern British Columbia, Canada; Vrije Universiteit Amsterdam, the Netherlands

Data sets and methods

Greenhouse gases

Estimated concentrations from 1750 are used to represent pre-industrial conditions. Calculations assume a pre-industrial mole fraction of 278 ppm for CO_2, 722 ppb for CH_4 and 270 ppb for N_2O.

World Data Centre for Greenhouse Gases operated by Japan Meteorological Agency https://gaw.kishou.go.jp/ .

World Meteorological Organization (WMO). WMO Greenhouse Gas Bulletin – No.17: The State of Greenhouse Gases in the Atmosphere Based on Global Observations through 2020.Geneva, 2021. https://library.wmo.int/index.php?lvl=notice_display&id=21975

World Ozone and Ultraviolet Radiation Data Centre operated by Environment and Climate Change Canada https://woudc.org/home.php .

Temperature

Global mean temperature series

The method for calculating global mean temperature anomalies relative to an 1850–1900 baseline has been updated since the State of the Global Climate 2020 report. The method was updated to take advantage of the assessment of long-term change and its uncertainty made by Working Group I in its contribution to the IPCC Sixth Assessment Report. The new method also makes use of a wider range of shorter data sets that are routinely updated to provide an authoritative assessment of recent temperature changes.

In the 2020 report (and earlier reports), changes relative to the 1850–1900 baseline were based on the HadCRUT4 data set which was the only data set that extended back to 1850. Other data sets were offset to match the average of HadCRUT4 over the period 1880–1900 (NASA GISTEMP and NOAA GlobalTemp) or 1981–2010 (ERA5, JRA-55).

In 2021, the IPCC Sixth Assessment Report Working Group I assessed change from 1850–1900 to other periods based on an average of four data sets – HadCRUT5, Berkeley Earth, NOAA–Interim and Kadow et al. (2020) – which all extend back to 1850. They assessed uncertainty by considering the range from the four estimates, taken from the lower bound of the uncertainty range of the coolest data set to the upper bound of the uncertainty range of the warmest. By making use of four data sets that extend back to 1850, Working Group I was able to make a more comprehensive estimate of uncertainty.

As two of the four IPCC data sets are not regularly updated, in the present report the estimate made by the IPCC for the temperature change between 1850–1900 and 1981–2010 is combined with estimated changes between 1981–2010 and the current year from six data sets to calculate anomalies for 2021 relative to 1850–1900.

There is good, though not perfect, agreement between the six data sets on changes from 1981–2010 to the present, as this is a period with good observational coverage. The additional modest uncertainty from the spread of the six data sets is combined with that of the IPCC's estimate of the uncertainty in the change from 1850–1900 to 1981–2010.

More precisely, six data sets (cited below) were used in the calculation of global temperature. Global mean temperature anomalies were calculated relative to an 1850–1900 baseline using the following steps:

1. The starting point was a time series of global monthly mean temperatures for each data set, as provided by the data providers. The anomalies were presented on different baselines.
2. For each data set, anomalies were calculated relative to the 1981–2010 average by subtracting the average for the period 1981–2010 for each month separately
3. An annual average was calculated from the available monthly averages.
4. The amount 0.69 °C was added to each series, based on the estimated difference between 1850–1900 and 1981–2010, calculated using the method from the IPCC Sixth Assessment Report Working Group I (the number is provided in the caption for Figure 1.12 in that report).
5. The mean and standard deviation of the six estimates were calculated.
6. The uncertainty in the IPCC estimate was combined with the standard deviation, assuming the two are independent and assuming the IPCC uncertainty range (0.54 °C to 0.79 °C) is representative of a 90% confidence range (1.645 standard deviations).

The number quoted in this report for 2022 (1.15 ± 0.13 °C) was calculated in this way with 1.15 °C being the mean of the six estimates.

Annual temperature maps

The method for calculating the map of annual temperature anomalies has also been updated. In the 2020 report, a map showing anomalies relative to 1981–2010 from a single data set (ERA5) was used. While the map was based on a single data set, the accompanying assessment was based on all available data sets.

For the map of temperature anomalies for 2022, a median value of six data sets was used (the same set used for the global mean) regridded to the spatial grid of the lowest resolution data sets (NOAAGlobalTemp and HadCRUT5 data sets), which are presented on a 5° latitude by 5° longitude grid. The median is used in preference to the mean to minimize the effect of potential outliers in individual grid cells. The half-range of the data sets provides an indication of the uncertainty. The spread between the data sets is largest at high latitudes and in Central Africa, both regions with sparse data coverage.

The following six data sets were used:

Berkeley Earth: Rohde, R. A.; Hausfather, Z. The Berkeley Earth Land/Ocean Temperature Record. Earth System Science Data 2020, 12, 3469–3479. https://doi.org/10.5194/essd-12-3469-2020

ERA5: Hersbach, H.; Bell, B.; Berrisford, P. et al. The ERA5 global reanalysis. Quarterly Journal of the Royal Meteorological Society 2020, 146 (730), 1999–2049. https://doi.org/10.1002/qj.3803

GISTEMP v4: GISTEMP Team, 2022: GISS Surface Temperature Analysis (GISTEMP), version 4.NASA Goddard Institute for Space Studies, https://data.giss.nasa.gov/gistemp/. Lenssen, N.;Schmidt, G.; Hansen, J. et al. Improvements in the GISTEMP Uncertainty Model. Journal of Geophysical Research: Atmospheres 2019, 124 (12): 6307–6326. https://doi.org/10.1029/2018JD029522

HadCRUT.5.0.1.0: Morice, C. P.; Kennedy, J. J.; Rayner, N. A. et al. An Updated Assessment of Near-Surface Temperature Change From 1850: The HadCRUT5 Data Set. Journal of Geophysical Research: Atmospheres 2021, 126 (3), e2019JD032361. https://doi.org/10.1029/2019JD032361 . HadCRUT.5.0.1.0 data were obtained from http://www.metoffice.gov.uk/hadobs/hadcrut5 on 21 October 2022 and are © British Crown Copyright, Met Office 2021, provided under an Open Government License, http://www.nationalarchives.gov.uk/doc/open-government-licence/version/3/

JRA-55: Kobayashi, S.; Ota, Y.; Harada, Y. et al. The JRA-55 Reanalysis: General Specifications and Basic Characteristics. Journal of the Meteorological Society of Japan.Ser. II 2015, 93 (1), 5–48. https://doi.org/10.2151/jmsj.2015-001, https://www.jstage.jst.go.jp/article/jmsj/93/1/93_2015-001/_article.

NOAAGlobalTemp v5: Zhang, H.-M., et al., NOAA Global Surface Temperature Dataset (NOAAGlobalTemp), Version 5.0. NOAA National Centers for Environmental Information. doi:10.7289/V5FN144H.

Huang, B.; Menne, M. J.; Boyer, T. et al. Uncertainty Estimates for Sea Surface Temperature and Land Surface Air Temperature in NOAAGlobalTemp Version 5. Journal of Climate 2020, 33 (4), 1351–1379. https://journals.ametsoc.org/view/journals/clim/33/4/jcli-d-19-0395.1.xml

Ocean heat content

Data used for estimates up to 2021:

Cheng, L.; Trenberth, K. E.; Fasullo, J. et al. Improved estimates of ocean heat content from 1960 to 2015, Science Advances 2017, 3 (3), e1601545. https://doi.org/10.1126/sciadv.1601545

Ishii, M.; Fukuda, Y.; Hirahara, S. et al. Accuracy of Global Upper Ocean Heat Content Estimation Expected from Present Observational Data Sets. SOLA 2017, 13, 163–167. https://doi.org/10.2151/sola.2017-030

Lyman, J. M.; Johnson, G. C. Estimating Global Ocean Heat Content Changes in the Upper 1800 m since 1950 and the Influence of Climatology Choice. Journal of Climate 2014, 27 (5), 1945–1957. https://doi.org/10.1175/JCLI-D-12-00752.1

von Schuckmann, K.; Le Traon, P.-Y. How well can we derive Global Ocean Indicators from Argo data? Ocean Science 2011, 7 (6), 783–791. https://doi.org/10.5194/os-7-783-2011.

In addition, data used up to 2020:

Desbruyères, D. G.; Purkey, S. G.; McDonagh, E. L. et al. Deep and abyssal ocean warming from 35 years of repeat hydrography, Geophysical Research Letters 2016, 43 (19), 310–356. https://doi.org/10.1002/2016GL070413

Gaillard, F.; Reynaud, T.; Thierry, V. et al. In Situ–Based Reanalysis of the Global Ocean Temperature and Salinity with ISAS: Variability of the Heat Content and Steric Height, Journal of Climate 2016, 29 (4), 1305–1323. https://doi.org/10.1175/JCLI-D-15-0028.1

Hosoda, S.; Ohira, T.; Nakamura, T. A monthly mean dataset of global oceanic temperature and salinity derived from Argo float observations. JAMSTEC Report of Research and Development 2008, 8, 47–59. https://www.jstage.jst.go.jp/article/jamstecr/8/0/8_0_47/_article

Kuusela M.; Stein, M. L. Locally stationary spatio-temporal interpolation of Argo profiling float data. Proceedings of the Royal Society A 2018, 474, 20180400. http://dx.doi.org/10.1098/rspa.2018.0400

Levitus, S.; Antonov, J. I.; Boyer, T. P. et al. World Ocean heat content and thermosteric sea level change (0-2 000 m) 1955–2010. Geophysical Research Letters 2012, 39 (10), L10603. https://doi.org/10.1029/2012GL051106

Li, H.; Xu, F.; Zhou, W. et al. Development of a global gridded Argo data set with Barnes successive corrections, Journal of Geophysical Research: Oceans 2017, 122 (2), 866–889, https://doi.org/10.1002/2016JC012285

Roemmich, D.; Gilson, J. The 2004–2008 mean and annual cycle of temperature, salinity, and steric height in the global ocean from the Argo Program, Progress in Oceanography 2009, 82 (2), 81–100. https://doi.org/10.1016/j.pocean.2009.03.004

von Schuckmann, K.; Le Traon, P. -Y.; Smith, N. et al., Eds. Copernicus Marine Service Ocean State Report, Journal of Operational Oceanography 2018, 11, S1–S142. https://doi.org/10.1080/1755876X.2018.1489208

Sea level

GMSL from CNES/Aviso+ https://www.aviso.altimetry.fr/en/data/products/ocean-indicators-products/mean-sea-level/data-acces.html#c12195

Marine heatwave and marine cold-spell data

MHWs are categorized as *moderate* when the sea-surface temperature (SST) is above the 90th percentile of the climatological distribution for five days or longer; the subsequent categories are defined with respect to the difference between the SST and the climatological distribution average: *strong*, *severe*, or *extreme*, if that difference is, respectively, more than two, three or four times the

difference between the 90th percentile and the climatological distribution average (Hobday et al., 2018). MCS categories are analogous but counting days below the 10th percentile.

The baseline used for MHWs and MCSs is 1982–2011, which is shifted by one year from the standard normal period of 1981–2010 because the first full year of the satellite SST series on which it is based is 1982.

Hobday, A.J. et al., 2018: Categorizing and Naming Marine Heatwaves. Oceanography, 31(2): 1–13. doi: https://eprints.utas.edu.au/27875/.

NOAA OISST v2: Optimum Interpolation Sea Surface Temperature (OISST):

Banzon, V. et al., 2016: A Long-Term Record of Blended Satellite and in Situ Sea-Surface Temperature for Climate Monitoring, Modeling and Environmental Studies. Earth System Science Data, 8(1): 165–176. doi: https://essd.copernicus.org/articles/8/165/2016/

Sea ice

Data set background: The sea ice section uses data from the EUMETSAT OSI SAF Sea Ice Index v2.1 (OSI-SAF, based on Lavergne et al., 2019 - https://osisaf-hl.met.no/v2p1-sea-ice-index) and the NSIDC v3 Sea Ice Index (Fetterer et al., 2017). Sea ice concentrations are estimated from microwave radiances measured from satellites. Extent is calculated as the area of ocean grid cells where the sea-ice concentration exceeds 15%. Although there are relatively large differences in the absolute extent between data sets, they agree well on the year-to-year changes and the trends. In this report, NSIDC values are reported for absolute extents (e.g. “18.95 million km2”) for consistency with earlier reports, while rankings are reported for both data sets.

Greenland ice sheet

Greenland ice sheet mass balance data are reported from three sources. Modelled changes in surface mass balance and total mass balance from 1985 to 2021 are based on the average of three regional climate and mass balance models, described in Mankoff et al. (2021). An alternative estimate of 2021 mass balance is given in the NOAA Arctic Report Card (Moon et al., 2021), based on satellite observations of melt area and surface mass balance models driven by the PROMICE surface weather station network. Satellite gravity data of total ice sheet mass balance from the GRACE and GRACE-FO missions are available from Wiese et al. (2019, updated to 2021). These data are available for both the Greenland and Antarctic ice sheets.

Mankoff, K. D.; Fettweis, X.; Langen, P. L. et al. Greenland ice sheet mass balance from 1840 through next week. Earth System Science Data 2021, 13 (10), 5001–5025. https://doi.org/10.5194/ essd-13-5001-2021.

Moon, T. A.; Tedesco, M.; Box, J. E. et al. Greenland Ice Sheet. In Arctic Report Card 2021; Moon, T. A.; Druckenmiller, M. L.; Thoman, R. L., Eds.; National Oceanic and Atmospheric Administration, 2021. https://doi.org/10.25923/546g-ms61.

Wiese, D.N.; Yuan, D. -N; Boening, C. et al. 2019. JPL GRACE and GRACE-FO Mascon Ocean, Ice, and Hydrology Equivalent Water Height RL06M CRI Filtered Version 2.0, Ver. 2.0, PO.DAAC, CA, USA. http://dx.doi.org/10.5067/TEMSC-3MJ62.

Precipitation

These GPCC data sets were used in the analysis:

- First Guess Monthly, DOI: 10.5676/DWD_GPCC/FG_M_100

- Monitoring Product (Version 2022), DOI: 10.5676/DWD_GPCC/MP_M_V2022_100
- Full Data Monthly (Version 2022), DOI: 10.5676/DWD_GPCC/FD_M_V2022_100
- Precipitation Climatology (Version 2022), DOI: 10.5676/DWD_GPCC/CLIM_M_V2022_100